Long-Range Segregation Phenomena in Shape-Selected Bimetallic Nanoparticles: Chemical State Effects

Mahdi Ahmadi,[†] Farzad Behafarid,[†] Chunhua Cui,[‡] Peter Strasser,[‡] and Beatriz Roldan Cuenya[†,§,*]

[†]Department of Physics, University of Central Florida, Orlando, Florida 32816, United States, [‡]Department of Chemistry, Chemical Engineering Division, Technical University Berlin, Berlin, Germany, and [§]Department of Physics, Ruhr-University Bochum, Bochum, Germany

ABSTRACT A study of the morphological and chemical stability of shape-selected octahedral $Pt_{0.5}Ni_{0.5}$ nanoparticles (NPs) supported on highly oriented pyrolytic graphite (HOPG) is presented. *Ex situ* atomic force microscopy (AFM) and *in situ* X-ray photoelectron spectroscopy (XPS) measurements were used to monitor the mobility of $Pt_{0.5}Ni_{0.5}$ NPs and to study long-range atomic segregation and alloy formation phenomena under vacuum, H_2, and O_2 environments. The chemical state of the NPs was found to play a pivotal role in their surface composition after different thermal treatments. In particular, for these *ex situ* synthesized NPs, Ni segregation to the NP surface was observed in all environments as long as PtO_x species were present. In the presence of oxygen, an enhanced Ni surface segregation was observed at all temperatures. In contrast, in hydrogen and vacuum, the Ni outward segregation occurs only at low temperature (<200−270 °C), while PtO_x species are still present. At higher temperatures, the reduction of the Pt oxide species results in Pt diffusion toward the NP surface and the formation of a Ni−Pt alloy. A consistent correlation between the NP surface composition and its electrocatalytic CO oxidation activity was established.

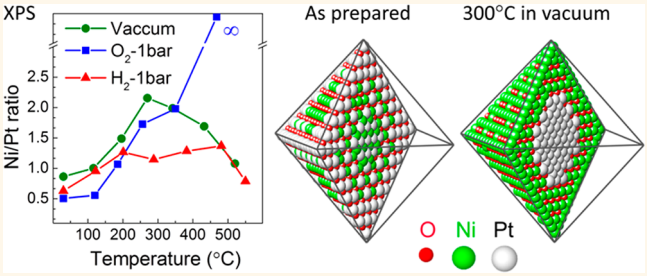

KEYWORDS: PtNi · octahedral · nanoparticle · segregation · diffusion · PtNi alloy · AFM · XPS

Bimetallic catalysts have numerous advantages as compared to their monometallic counterparts, such as enhanced activity, selectivity, and durability.[1] For instance, when combined with secondary metals (M) such as Ni, Fe, Cu, Co, or Ti, increased activities have been observed for Pt-based catalysts in oxygenate reforming reactions,[2−5] the oxygen reduction reaction (ORR),[6−11] hydrogenation reactions,[12,13] CO oxidation,[14−16] and CH_4 reforming.[17,18] In all of these applications, the manipulation of the geometrical and electronic properties of the resulting alloy, in particular, the Pt−Pt bond length (strain effects) and the position of the d-band center are considered to play a key role in the unusual properties displayed by the bimetallic systems.

A variety of methods have been employed for the synthesis of bimetallic nanoparticle (NP) catalysts, with special focus dedicated to improving their activity and stability under reaction conditions in different gaseous or liquid (electrochemical) environments.[7,11,19−24] Changes in their structure and surface composition, leaching and dissolution of a given element, as well as coarsening are the main factors responsible for the loss in the activity of these catalysts.[25−27] Decreased NP mobility and sintering have been achieved for Pt-based catalysts through alloying with Co, Fe, and Ni.[25,26,28] Although dissolution of Pt-based catalysts in acidic environments is commonly described as a negative characteristic leading to a decrease in activity,[29,30] in certain cases it was reported to result in improved catalytic performance *via* the increase of the surface roughness.[31−33]

Overall agreement exists on the importance of the structure of the bimetallic alloys. Segregation phenomena or alloy formation processes in bimetallic systems are determined by the interplay between the surface energy of each element, their atomic radius, and the chemical ordering energy [difference in energy between structures with (i) a periodic appearance of the two elements in the lattice and (ii) the completely disordered analog with randomly

* Address correspondence to beatriz.roldan@rub.de.

Received for review July 22, 2013 and accepted September 9, 2013.

Published online September 09, 2013
10.1021/nn403793a

positioned elements].[34] In general, a higher ordering energy is expected to hinder segregation processes.[34] Based on the phase diagram of bulk PtNi alloys, $Pt_{0.5}Ni_{0.5}$ has a chemically disordered FCC structure above its order−disorder transition temperature, T_C^{bulk} = 900 K, and a chemically ordered $L1_0$ phase below that temperature.[35] However, for nanoparticles T_C^{NP} might differ from T_C^{bulk}, depending on the NP size and shape.[36] The degree of chemical ordering of an alloyed NP is expected to drastically affect its segregation behavior. For instance, while in a chemically disordered system, the segregation process is a smooth function of the NP stoichiometry (Pt/Ni ratio); in an ordered system, the segregation behavior could vary significantly with only slight changes in the stoichiometry, for example, for $Pt_{0.50}Ni_{0.50}$ *versus* $Pt_{0.51}Ni_{0.49}$ and $Pt_{0.49}Ni_{0.51}$.[34] In addition, while a chemically ordered structure may be thermodynamically favorable for an equiatomic composition at room temperature, depending on the NP growth kinetics, the chemical structure of bimetallic NPs could be initially disordered and remain disordered until it is treated at high temperature.[37−39] Usually, the presence of oxidized species or inhomogeneities in the initial elemental distribution of NPs leads to chemically disordered systems. Also, the phase diagram, the order−disorder transition temperature, and the atomic segregation behavior of clean bimetallic NPs is likely distinct from that of the corresponding oxidized or adsorbate-covered NPs.[36,40]

Sandwich structures with thin Pt overlayers deposited on 3d-metal surfaces [Pt-3d-Pt(111)] have been proven to be more effective catalysts than pure Pt for low-temperature hydrogenation reactions,[12,13,41] while for oxygenate reforming processes, 3d-metal overlayers on Pt surfaces [3d-Pt-Pt(111)] displayed the greatest activity.[42,43] In the realm of electrocatalysis, a (111) oriented Pt_3Ni surface, thermally segregated into a Pt skin structure was found to be the most active structure for the electrocatalytic reduction of molecular oxygen to water.[6] In contrast, the electrocatalytic oxidation of CO or small organic molecules is most efficiently catalyzed by Pt−Ru and Pt−Sn alloys.[44]

More importantly, the structure of the catalysts might change depending on the reaction conditions, making *in situ* and *operando* studies crucial for the understanding of structure−reactivity correlations in material systems prone to segregation. For example, by annealing a 3d metal-Pt-Pt(111) structure in vacuum, Pt was found to surface segregate, turning this material from an effective oxygenate reforming into a hydrogenation catalyst.[42,45] On the other hand, 3d-metal-Pt-Pt structures were the most stable in oxygen environments. Surface segregation of Pt was observed experimentally for PtRu NPs in a H_2 environment[46] and theoretically predicted for Pt−M (Ni, Re, Mo) NPs.[36,47] Annealing PtCo NPs treated in acid solutions also lead to Pt surface segregation and the formation of sandwich-Pt structures.[10]

The current study focuses on the *in situ* evolution of the structure and surface composition of shape-selected octahedral Pt−Ni NPs under different chemical environments (O_2, H_2, vacuum). This material system is of interest due to its use in a broad range of industrial catalysis applications. Owing to the exclusive exposure of (111)-oriented facets, it has been touted as an ideal electrocatalysts for the electroreduction of oxygen.[8,9,44,48−50] Even though among all 3d-metals Ni has the highest energy barrier for segregation,[51] the presence of adsorbates can drastically promote Ni surface segregation. Density functional theory (DFT) calculations showed low potential for Ni surface segregation in H, S, Se, or C environments due to their weak surface/subsurface bonding, while adsorbates such as O or N were found to promote segregation.[52] Reversible changes in the structure of (5−20 nm) Pt−Ni NPs prepared *via* deposition-precipitation were recently reported, with Ni-surface enrichment in oxygen and Pt-richer surfaces in H_2 after annealing at 300 °C.[53]

Our work describes the morphological stability and atomic segregation phenomena in size- and shape-selected octahedral Pt−Ni NPs supported on highly ordered pyrolytic graphite (HOPG), with emphasis on the influence of pre-existing oxides on the segregation trends observed. The NP shape was resolved by transmission electron microscopy (TEM). *In situ* X-ray photoelectron spectroscopy (XPS) and *ex situ* atomic force microscopy (AFM) were used to monitor the effect of diverse gaseous environments on the structure and surface composition of $Pt_{0.5}Ni_{0.5}$ alloy NPs. Three differently pretreated (vacuum, hydrogen, and oxygen at 300−350 °C) PtNi NP samples were used to demonstrate the effect of surface composition on catalytic reactivity for the electro-oxidation of CO. The results from catalytic CO stripping measurements were found to be fully consistent with the XPS-derived Ni surface segregation and PtNi alloying trends in the three environments.

RESULTS AND DISCUSSION

Figure 1 shows a TEM image of ~9 nm $Pt_{0.5}Ni_{0.5}$ NPs in an as-prepared sample. The PtNi NPs show a narrow size distribution and a consistent octahedron shape. Figure 2 displays *ex situ* AFM images of three identically prepared fresh octahedral PtNi NP/HOPG samples (a−c), together with images acquired at room temperature (RT) after annealing at 150 °C (d−f) and 250 °C (g−i). The first column displays pictures acquired after annealing in vacuum, the second column after H_2, and the third column after O_2. Initially (fresh samples) the NPs are homogenously dispersed over the entire support surface. Annealing in vacuum leads

to a progressive decrease of the average NP size without significant sintering, although a less homogeneous coverage of the support surface by the NPs is observed. In contrast, identical treatments in H_2 and O_2 lead to enhanced NP mobility, and the preferential decoration of HOPG steps already at 150 °C. Under oxygen, a lower density of NPs on HOPG terraces is observed at all temperatures as compared to hydrogen, suggesting enhanced atomic (Ostwald ripening) and NP (diffusion-coalescence) mobility. In addition, agglomeration of NPs is observed on certain support regions after the treatment in O_2, with other areas showing large uncoated voids. According to ref 54, in the case of pure Ni NPs, preferential bonding to oxidized and defect sites on HOPG was observed, which might explain the inhomogeneous NP dispersion on the support. Enhanced NP mobility was also seen under H_2 as compared to vacuum. Such facile movement is assigned to a weak binding of the $Pt_{0.5}Ni_{0.5}$ NPs to the HOPG support. Following related literature,[55−58] a very distinct behavior, for example, lower atomic/NP mobility, might have been observed if these NPs would have been supported on an oxide substrate,[55,56] where at low temperature and under oxidizing conditions a stronger oxidized metal NP/support is formed. On the weakly binding graphite, the exposure to either H_2 or O_2 seems to contribute to the destabilization of the NPs.

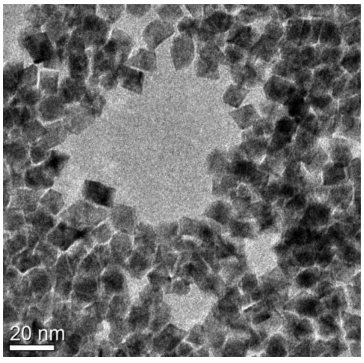

Figure 1. TEM image of octahedral PtNi NPs.

XPS spectra from the Pt-4f (a−c) and Ni-2p (d−f) core level regions are shown in Figure 3 after annealing treatments in vacuum (a,d), 1 bar of H_2 (b,e), and 1 bar of O_2 (c,f). In agreement with literature references,[59−61] the Pt-4f XPS data were fitted with three doublets corresponding to metallic Pt ($4f_{7/2}$, 71.2 eV), Pt^{2+} ($4f_{7/2}$, 72.4 eV), and Pt^{4+} ($4f_{7/2}$, 73.7 eV). The Ni-2p region was also fitted with three double peaks assigned to metallic Ni ($2p_{3/2}$, 852.5 eV), Ni^{2+} ($2p_{3/2}$, 855−856.2 eV), and satellite features (861, 878.2 eV).[62−64] The evolution of the oxidation state of the PtNi NPs is shown in Figure 4.

The *ex situ* prepared $Pt_{0.5}Ni_{0.5}$ NPs were initially composed of a significant fraction of Ni^{2+} species

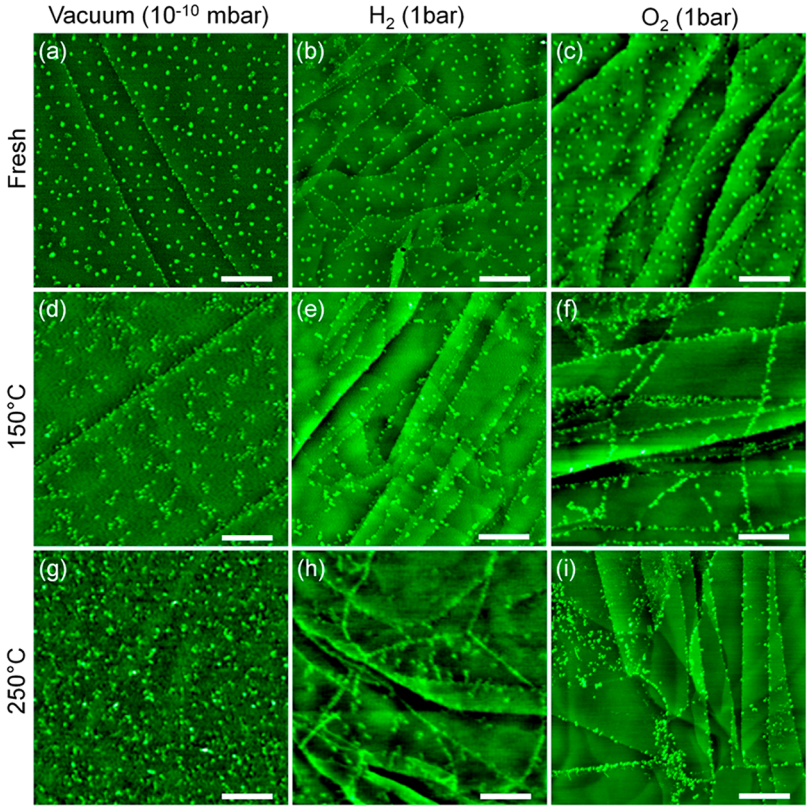

Figure 2. AFM images of octahedral PtNi NPs supported on HOPG acquired at *ex situ* (air) at RT after the treatments indicated. Scale bars in all images are 400 nm.

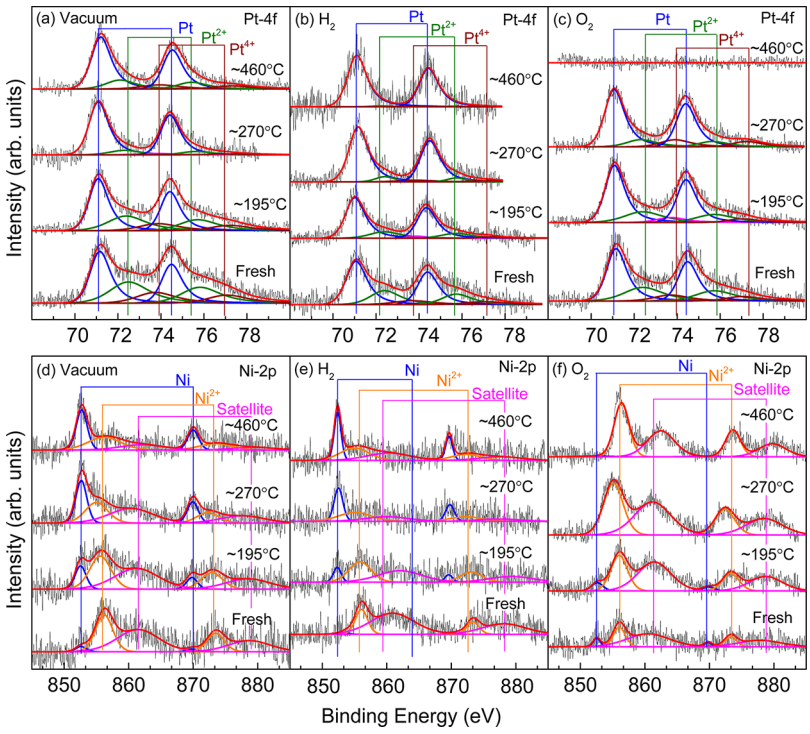

Figure 3. XPS spectra from the (a−c) Pt-4f and (d−f) Ni-2p core level regions of PtNi NPs supported on HOPG acquired at RT as prepared (fresh) and after annealing in vacuum and in 1 bar of O_2 and H_2 for 20 min at the indicated temperatures.

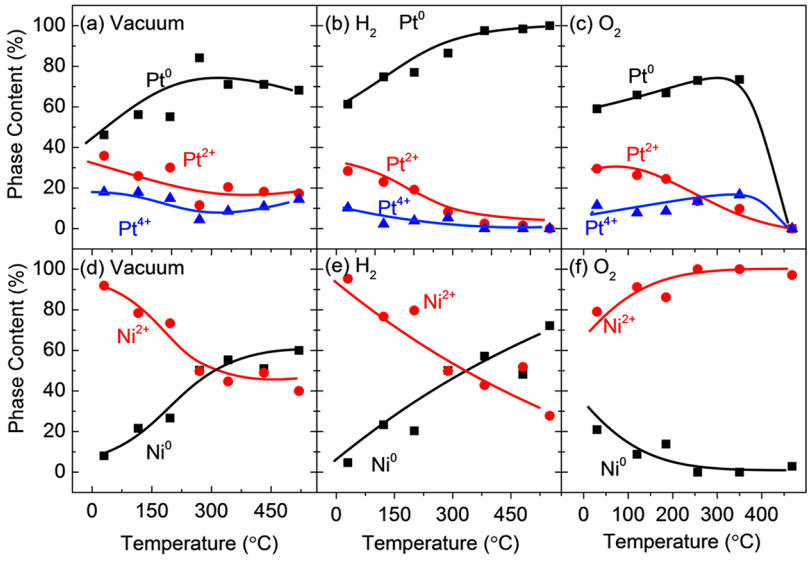

Figure 4. Relative content of (a−c) Pt and (d−f) Ni species extracted from the analysis of XPS data acquired after annealing in vacuum (a,d), 1 bar of H_2 (b,e), and 1 bar of O_2 (c,f).

(NiO or NiOH, ~80−95%), with Pt also partially oxidized [40−50% Pt^{2+} and Pt^{4+} in the form of PtO/PtO_2 or $Pt(OH)_{2x}$],[65,66] Figure 4. Annealing in hydrogen up to 460 °C only led to the partial reduction of the Ni^{2+} species (~45%), with significant Pt reduction above 270 °C, but a small PtOx component still observed at 460 °C. A faster reduction of the PtOx species in the 200−460 °C temperature range was detected during the annealing in H_2 as compared to vacuum. Annealing in oxygen resulted in a progressive increase in the Ni^{2+} content, with partial decomposition of the $Pt^{\delta+}$ species up to 270 °C, and the complete loss of the Pt signal at 460 °C, Figure 3c.

The Ni/Pt atomic ratio after the thermal treatment under the different gaseous atmospheres is shown in Figure 5. In the absence of adsorbates, due to the larger atomic radius of Pt and despite its slightly higher surface energy (2.475 J/m^2) as compared to Ni (2.45 J/m^2),[67] Pt segregation to the NP surface is expected.[34,36] Although it has been shown that the

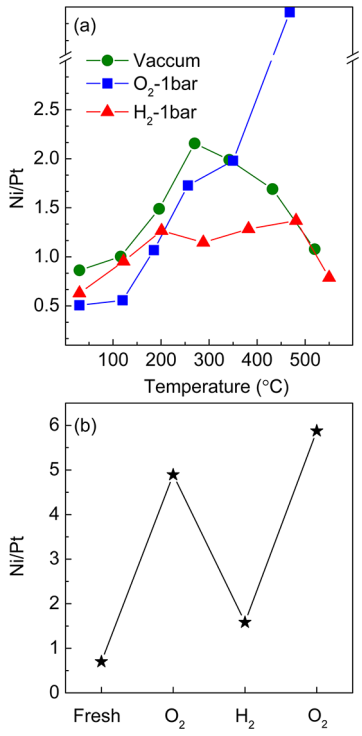

Figure 5. (a) Ni/Pt atomic ratios extracted from XPS measurements acquired at RT after annealing in O_2 (1 bar), H_2 (1 bar), and vacuum at the indicated temperatures. (b) Ni/Pt ratio after NP annealing at 450 °C in O_2 and H_2 environments at low pressure (5×10^{-6} mbar), showing the reversibility of the segregation/alloying process.

size, shape, and stoichiometry of the NPs affect their segregation behavior,[36,68] consensus exists regarding the formation of Pt-rich overlayers on (111) and (100) surfaces in cases where segregation takes place.[34,36,69,70] However, such segregation is limited only to the first few atomic layers at the surface, commonly resulting in the formation of a Pt skin or sandwich structure, in which the first atomic layer is Pt-rich and the second layer is Ni-rich. Such structure might be achieved through a short-range atomic exchange near the surface, with Pt atoms in the second layer switching places with their neighboring Ni atoms at the surface. However, the small changes in the Pt and Ni signals brought about by the formation of the Pt skin might not be detectable with common laboratory XPS systems (1486.6 eV X-rays in this case). This is due to the small contribution of the topmost surface layers considering the photoelectron inelastic mean free paths involved (~1.8 nm for Pt photoelectrons and ~1 nm for Ni). Here we should highlight that such short-range segregation should not be confused with the long-range segregation that would result in phase-separation or core–shell structure formation reported for other systems.[33,71,72] In most cases, long-range segregation phenomena occur for systems in which the two metals have a different crystalline structure, such as Pt–Ru with fcc and hcp structures, respectively, or Fe–Au with bcc and fcc structures, which is not the case for Pt–Ni (both fcc).

In the present study, an increase in the Ni/Pt ratio was observed for our samples in vacuum and in H_2 at low temperature (<270 °C in vacuum and <200 °C in H_2, remaining subsequently stable up to 460 °C in H_2). This trend is assigned to the initial chemical state of the *ex situ* prepared NPs, which was characterized by the presence of oxygen at surface/subsurface regions. Due to the much higher affinity of Ni for oxygen as compared to Pt (NiOx formation energy of −2.54 eV per O *vs* PtO, PtO_2 formation energies of −0.41 and −0.63 eV per O),[73] Ni surface segregation is observed under reducing atmospheres until significant oxygen removal (oxide decomposition) is achieved, which was found to occur here above 270 °C in vacuum and above 200 °C in H_2.

In vacuum, a change in the Ni/Pt ratio is observed, with a drastic decrease above 270 °C. The same phenomenon is not seen under hydrogen until 460 °C, with the Ni/Pt ratio continuously increasing up to 200 °C, and then remaining nearly constant from 200 °C to 460 °C, until a drop in the Ni/Pt ratio is finally observed at 550 °C. The strong reduction of the Ni/Pt ratio observed at high temperature is assigned to the interdiffusion of reduced Pt and Ni species and the formation of a homogeneous PtNi alloy.

The Ni surface segregation taking place when oxygen is present on the NP surface is considered to proceed *via* the replacement of Pt atoms in surface PtOx species by Ni. Such a trend explains our experimental results showing different temperature regimes for the changeover from Ni surface segregation to Pt–Ni interdiffusion in different environments (*i.e.* vacuum *vs* H_2), primarily depending on the temperature required for the full removal of PtO_x species, and secondarily by the continuous depletion of O from Ni-rich NP regions. The reduction of the PtO_x species at low temperature was found to stop the Ni outward segregation and at high temperature, the reduction of Ni oxide species results in Pt–Ni intermixing through alloy formation. The former arguments explain why the Ni/Pt ratio does not increase in H_2 as much as in vacuum due to the earlier reduction of the PtO_x species in H_2, which hinders the segregation of Ni. The later illustrates the lack of change of the Ni/Pt ratio between 200 and 460 °C in H_2, since the more drastic Ni reduction, favoring the alloy formation, occurs at higher temperature (≥500 °C).

When the samples are annealed in oxygen, the progressive segregation of Ni to the NP surface and the concomitant formation of NiO species was detected, with a drastic increase in the Ni/Pt ratio above 350 °C, and the complete disappearance of the Pt signal in XPS at 460 °C, Figure 5(a). The loss of the Pt signal could be attributed to (i) its inward segregation (toward the NP core), with the Pt XPS signal being

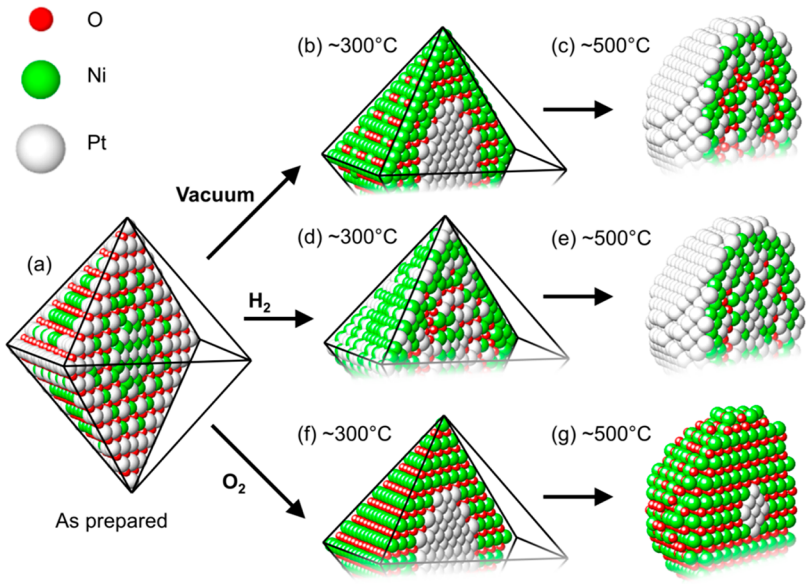

Figure 6. Schematic models describing the segregation of Pt and Ni atoms in octahedral $Pt_{0.5}Ni_{0.5}$ NPs (a) as-prepared and after annealing from 25 to 500 °C in the following environments: (b, c) vacuum (10^{-10} mbar), (d, e) H_2 (1 bar), and (f, g) O_2 (1 bar).

suppressed by the presence of the overlaying Ni shell, or (ii) the loss of Pt in the form of volatile PtO_2 compounds. In order to corroborate the likelihood of the first scenario, the inelastic mean free path (IMFP) of Pt-4f photoelectrons in Ni (~1.9 nm) should be compared to the thickness of the NiO shell. For $Pt_{0.5}Ni_{0.5}$ NPs of our initial size, the IMFP is not expected to be much smaller than the NiOx shell thickness, and therefore, no substantial damping of the Pt XPS signal should have been observed, provided that no significant sintering takes place during the annealing treatment in oxygen at 460 °C, as observed *via* AFM. The second scenario, namely, that involving the loss of Pt is more likely. Nevertheless, such possibility should also be cautiously considered, because the NiO shell formed under these conditions might serve to protect the Pt at the NP core. However, it is plausible that the Pt atoms have enough mobility at high temperature to reach the NP surface and desorb as PtO_2 after coming into contact with oxygen. The latter effect might explain the counterintuitive increase in the content of Pt^0 species with increasing temperature in oxygen, Figure 4c, due to PtO_x removal from the NP surface.

Figure 5b shows measurements carried out under O_2, H_2, and again O_2 at 450 °C at a pressure of 5×10^{-6} mbar, revealing that the segregation-alloying process is reversible. However, the slight decrease in the Ni/Pt ratio observed after the second annealing cycle hints toward a similar Pt loss in O_2 as described above for a higher O_2 pressure treatment (1 bar) through its volatilization as PtO_2.

Figure 6 schematically illustrates the atomic segregation trends extracted from our *in situ* XPS data. Figure 6a shows the as-prepared sample with a PtNi alloy in the core and Pt/Ni oxide species near the surface due to the exposure of the NPs to air after preparation. As was shown in our previous study,[49] the corners and edges of the NP are Pt-rich, while the facets are Ni-rich. This is a result of kinetic phenomena taking place during the NP synthesis. Annealing in vacuum up to ~300 °C results in Ni atoms exchanging their positions with Pt atoms in oxide species (mainly at and near the NP surface), leading to the formation of a Ni oxide shell and a Pt rich core. Both, Ni and Pt species get partially reduced within this temperature range, Figure 6b. Annealing in vacuum at higher temperatures (*e.g.* 500 °C) results in the reduction of Ni and the consequent interdiffusion of Pt and Ni atoms, leading to the formation of a uniform PtNi alloy, Figure 6c. The shape of the NPs is not expected to remain stable at these high temperatures, and therefore, the NPs are shown here with a truncated octahedron shape. In the case of the annealing in hydrogen, the reduction of Pt oxides occurs much earlier, and therefore, the Ni−Pt exchange is not as extensive as when the samples are annealed in vacuum, Figure 6d, as indicated by the lack of significant change in the Ni/Pt ratio within the 200−400 °C temperature range. At high temperature, the alloy formation in H_2 is similar to that observed in vacuum, with the exception of a more extensive $Ni^{\delta+}$ and $Pt^{\delta+}$ reduction, Figure 6e. Annealing in oxygen brings the Ni out toward the NP surface, resulting in a completely oxidized NiO shell, in contrast to the cases of annealing in vacuum and H_2, Figure 6f. At last, annealing in O_2 at high temperature (460 °C) was found to result in the partial or total loss of Pt *via* the formation of volatile PtO_2, with the NPs mainly composed of NiO species, Figure 6g. It should also be considered that our octahedral PtNi NPs are kinetically

formed, and thus, they do not represent the most thermodynamically stable shape. Therefore, at moderate temperatures (*e.g.*, 500 °C in the schematic of Figure 6), the loss of the octahedral shape is expected. Although truncated cubo-octahedral PtNi NPs were shown to have a slightly lower energy (0.003 eV per atom) than NPs with octahedral shape,[36] any conclusion on what shape should be experimentally observed should be considered with caution. Due to the presence of adsorbates or surface/subsurface oxides under common experimental conditions, the reconstruction on (100) facets, which is the main reason for the truncated cubo-octahedral shape to be the more thermodynamically favorable, is expected to be lifted.[36] Additionally, it should be noted that none of the NPs in our study are completely reduced, even after treatment at the highest temperature shown (460 °C), and therefore, any prediction of their shape should include their oxidation state as well. Thus, the final shape of a NP may vary after treatment in different environments depending on its oxidation state as well as on adsorbate-induced modifications of its surface energy.

The surface composition of a catalyst generally affects its catalytic reactivity. To demonstrate this for thermally treated $Pt_{0.5}Ni_{0.5}$ octahedral NPs, the electrocatalytic CO oxidation reaction was chosen. Catalyzed by the surface of the shaped Pt−Ni NPs, the electrochemical CO oxidation reaction involves the activation of water to surface OH followed by its reaction with adsorbed CO to CO_2. The reaction process proceeds according to

$$H_2O + * \rightarrow OH_{ad} + H^+ + e^- \quad (1)$$

$$CO_{ad} + OH_{ad} \rightarrow CO_2 + H^+ + e^- + 2* \quad (2)$$

where * denotes a surface site for water activation. Earlier CO stripping studies on PtNi NPs showed that there exist two types of water activation sites:[48] (i) surface Ni oxide sites that act as highly active water activation promoter sites, shifting the CO stripping peak toward a more cathodic electrode potential between 0.3 and 0.6 V/RHE (this potential range is shaded in Figure 7); (ii) Pt surface sites that may as well serve as water activation sites; however, these sites promote such process at more anodic potentials, and as a result of this, they yield anodic CO stripping charge in the potential range of 0.6−1.0 V/RHE, Figure 7.

CO electrooxidation (CO stripping) was carried out using a single anodic voltammetric potential sweep between 0.05 and 1.0 V/RHE, Figure 7. The first CO stripping cycle (red in Figure 7) was followed by a second baseline voltammetric cycle (black in Figure 7). The total charge of the difference between the black and the red voltammograms corresponds to the amount of electro-oxidized (and typically to the amount of initially adsorbed) surface CO. The recorded instantaneous Faradaic currents correspond to the CO

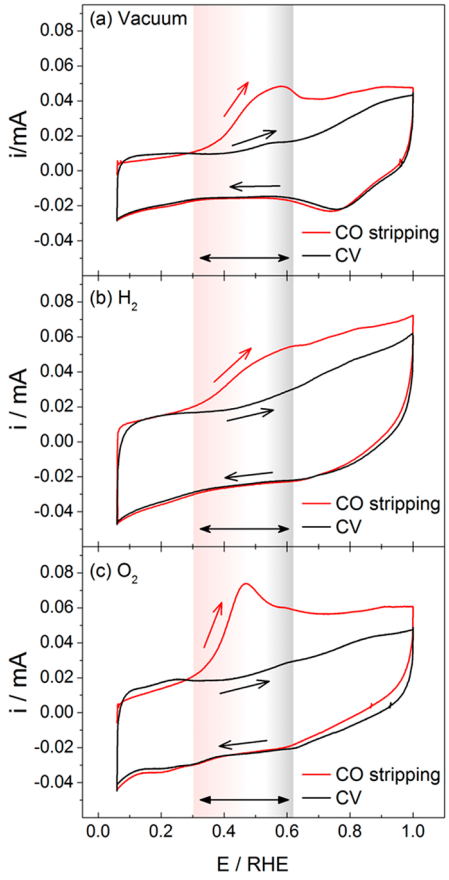

Figure 7. CO monolayer stripping voltammetry of octahedral $Pt_{0.5}Ni_{0.5}$ NPs after treatments under reactive gases and ultrahigh vacuum. The first stripping cycle is shown in red, the second baseline voltammetric cycle is shown in black, and scan directions are indicated by arrows: (a) 350 °C in vacuum, (b) 300 °C in H_2, and (c) 350 °C in O_2. Conditions: CO adsorption at 0.05 V/RHE, 50 mV/s, and 0.1 M KOH. The shaded potential range (0.3−0.58 V/RHE) indicates where CO stripping occurs by NiO_x-promoted water activation, eq 1 and ref 48.

oxidation reaction rate, while the CO oxidation peak potentials bear (often non trivial) relationships to CO and water chemisorption. Figure 7 displays the CO stripping voltammetry of one of the (a) vacuum-treated (350 °C), (b) hydrogen-treated (300 °C), and (c) oxygen-treated (350 °C) $Pt_{0.5}Ni_{0.5}$ NP catalyst samples. It is evident that the peak profiles of the three differently treated samples show characteristic differences. It is plausible that, given the otherwise identical experimental conditions, the observed differences in the CO oxidation profiles are linked to their different surface compositions after the distinct thermal pretreatments before the electrochemical measurements. To corroborate this hypothesis, we recall the earlier findings mentioned above regarding the CO stripping potentials and the presence of Ni oxide surface species.[48] CO oxidation charges, Q, were analyzed for the potential region associated with the presence of surface Ni oxides. The vacuum-annealed sample showed a Q value of 100 μC, while the

H_2- and O_2-treated samples showed charges of 88 and 160 μC, respectively. These values clearly suggest that the oxygen-treated NPs oxidize CO to a large extent under the promotion of surface Ni oxide species. The H_2-treated NPs, in contrast, appears to show the least Ni oxide promotion, associated with the most metallic surface Pt character, while the vacuum-treated NPs show an intermediate behavior. These conclusions are fully commensurate with the surface compositional discussion above based on XPS results and offer a consistent composition-activity relationship.

CONCLUSION

Size- and shape-selected octahedral NPs supported on HOPG have used as a model system to study atomic segregation phenomena in $Pt_{0.5}Ni_{0.5}$ NP catalyst under different gaseous environments (1 bar H_2, 1 bar O_2, and vacuum). Because of the presence of oxygen species on the *ex situ* prepared fresh samples and the high oxygen affinity of Ni, Ni segregation to the NP surface was observed in all environments at low temperature ($T < 200-270$ °C). Such a result is explained in terms of a place exchange replacement process of Pt in surface PtOx species by Ni. In vacuum, Ni surface segregation continued up to 270 °C, above which the segregation of Pt to the NP surface was observed. In H_2, Ni segregation (an increase in the Ni/Pt ratio) ceased as early as 200 °C, possibly attributable to the earlier reduction of surface oxide species under H_2 exposure. Subsequently, the Ni/Pt ratio remains nearly constant in H_2 between 200 and 460 °C, above which Pt-surface enrichment was detected. It is reasonable to assume that the formation of the stable PtNi alloy is responsible for the compositional plateau. Thermal treatments in oxygen lead to a drastic Ni surface segregation and the formation of NiO species. Under such an environment, a NP configuration with a thick NiO shell and a small PtNi alloy core was inferred, with Pt being lost as PtO_2 at or above 460 °C.

CO electrooxidation was used as a model reaction to demonstrate how the surface composition affects the catalytic reactivity of the shaped $Pt_{0.5}Ni_{0.5}$ NPs after pretreatment in different gaseous atmospheres within the 300−350 °C temperature range. Being a sensitive diagnostic tool for Ni oxide surface species, CO stripping voltammetry confirmed the predominant presence of Ni oxides in the O_2-treated NPs, a largely Pt metallic character of the H_2-treated NPs, and the intermediate state of the vacuum-annealed NPs.

Our study highlights the importance of the initial chemical state of the NPs, in particular, the presence of oxygen, on the subsequent NP structural and chemical stability and atomic segregation trends. Furthermore, it illustrates how different adsorbates, commonly present in catalyst break-in pretreatments under *operando* conditions, can affect the composition of their surface and near-surface regions, and therefore, also their reactivity.

EXPERIMENTAL SECTION

Octahedral Pt−Ni bimetallic NPs with a Pt/Ni ratio of 1:1 were prepared using wet-chemical methods (a solvothermal process at elevated pressure),[74] with dimethylformamide (DMF) serving as solvent, surfactant, and reducing agent.[7,8,49] The as-prepared solution was 5-fold diluted with isopropanol and drop-coated on HOPG substrates after 10 min of sonication. The dilution allowed a better dispersion and lack of agglomeration of the as-prepared NPs on the HOPG supports.

Transmission electron microscopy (TEM) images were obtained by a FEI TECNAI G2 20 S-TWIN transmission electron microscope with LaB6−cathode. The microscopy work was carried out with an accelerating voltage of 200 kV.

Thermal treatments in different environments were conducted in a high pressure (HP) reaction cell (SPECS GmbH). The HP cell was evacuated after each treatment and the samples transferred to the attached ultrahigh vacuum (UHV) system without exposure to air. The XPS measurements were acquired *in situ* using a monochromatic X-ray source (Al Kα, 1486.6 eV) operating at 350 W and a hemispherical electron analyzer (Phoibos 100, SPECS GmbH). For the XPS study, three identical $Pt_{0.5}Ni_{0.5}$ NP samples were isochronally annealed in 1 bar O_2, 1 bar H_2, and vacuum environments for 20 min at temperatures ranging from RT to 650 °C. All XPS spectra were measured at RT after the respective heating cycles. The high resolution XPS data were acquired using a pass energy, E_{pass}, of 18 eV. The XPS spectra were analyzed using the CASA XPS software.[75] All spectra were aligned using the C-1s peak from the graphite support at 284.3 eV as reference.

In order to extract information about the changes in the sample morphology, size, and dispersion of the $Pt_{0.5}Ni_{0.5}$ NPs under the different environments, three identical $Pt_{0.5}Ni_{0.5}$ NP samples were *in situ* annealed in 1 bar O_2, 1 bar H_2, and ultrahigh vacuum as described above. Subsequently, AFM measurements (Digital Instruments, Nanoscope III) were acquired *ex situ* at room temperature in tapping mode.

Thermally treated $Pt_{0.5}Ni_{0.5}$ NPs supported on HOPG were characterized with respect to their electrocatalytic oxidation of adsorbed CO monolayers during anodic potential scans ("CO stripping") in alkaline 0.1 M KOH electrolytes. This procedure has been routinely carried out to assess the CO oxidation activity of electrocatalysts or to determine the real surface area of a Pt electrocatalyst.[76−78] After bubbling the electrolyte with Ar at room temperature for 15 min to remove all traces of dissolved air, CO was bubbled for 15 min at an applied electrode potential of 0.05 V/RHE at which a stable saturated monolayer of adsorbed CO forms at the surface of the catalyst. Subsequently, under continued potential control at 0.05 V/RHE, dissolved CO was removed by bubbling Ar gas for another 15 min, such that only the adsorbed CO layer remained in the electrochemical system. Finally, the electrode potential was scanned at 50 mV/s from +0.05 to +1.0 V/RHE to record the CO electrooxidation. One additional potential cycle was conducted in order to record the value of the hydrogen underpotential deposition (H_{upd}) charge and to establish the electrochemical baseline of the $Pt_{0.5}Ni_{0.5}$ NP catalyst.

Conflict of Interest: The authors declare no competing financial interest.

Acknowledgment. We thank Dr. Lin Gan for his assistance with the acquisition of the TEM images. M.A., F.B., and B.R.C. acknowledge the financial support from the US National Science Foundation (NSF CHE-1213182). C.C. and P.S. were funded by a U.S. DOE EERE award (DE-EE0000458) *via* a subcontract

through General Motors. P.S. also acknowledges financial support through the cluster of excellence in catalysis (UniCat) funded by the DFG and managed by the TU Berlin.

REFERENCES AND NOTES

1. Sinflet, J. H. Bimetallic Catalysts—Discoveries. *Concepts and Applications*; John Wiley & Sons: New York, 1983.
2. Croy, J. R.; Mostafa, S.; Hickman, L.; Heinrich, H.; Roldan Cuenya, B. Bimetallic Pt-Metal Catalysts for the Decomposition of Methanol: Effect of Secondary Metal on the Oxidation State, Activity, and Selectivity of Pt. *Appl. Catal., A* **2008**, *350*, 207–216.
3. Orucu, E.; Gokaliler, F.; Aksoylu, A. E.; Onsan, Z. I. Ethanol Steam Reforming for Hydrogen Production Over Bimetallic Pt−Ni/Al_2O_3. *Catal. Lett.* **2008**, *120*, 198–203.
4. Stottlemyer, A. L.; Ren, H.; Chen, J. G. Reactions of Methanol and Ethylene Glycol on Ni/Pt: Bridging the Materials Gap between Single Crystal and Polycrystalline Bimetallic Surfaces. *Surf. Sci.* **2009**, *603*, 2630–2638.
5. Tanksale, A.; Beltramini, J. N.; Dumesic, J. A.; Lu, G. Q. Effect of Pt and Pd Promoter on Ni Supported Catalysts—A TPR/TPO/TPD and Microcalorimetry Study. *J. Catal.* **2008**, *258*, 366–377.
6. Stamenkovic, V.; Mun, B. S.; Mayrhofer, K. J. J.; Ross, P. N.; Markovic, N. M.; Rossmeisl, J.; Greeley, J.; Norskov, J. K. Changing the Activity of Electrocatalysts for Oxygen Reduction by Tuning the Surface Electronic Structure. *Angew. Chem., Int. Ed.* **2006**, *45*, 2897–2901.
7. Carpenter, M. K.; Moylan, T. E.; Kukreja, R. S.; Atwan, M. H.; Tessema, M. M. Solvothermal Synthesis of Platinum Alloy Nanoparticles for Oxygen Reduction Electrocatalysis. *J. Am. Chem. Soc.* **2012**, *134*, 8535–8542.
8. Cui, C.; Gan, L.; Li, H.-H.; Yu, S.-H.; Heggen, M.; Strasser, P. Octahedral PtNi Nanoparticle Catalysts: Exceptional Oxygen Reduction Activity by Tuning the Alloy Particle Surface Composition. *Nano Lett.* **2012**, *12*, 5885–5889.
9. Wu, J. B.; Zhang, J. L.; Peng, Z. M.; Yang, S. C.; Wagner, F. T.; Yang, H. Truncated Octahedral Pt_3Ni Oxygen Reduction Reaction Electrocatalysts. *J. Am. Chem. Soc.* **2010**, *132*, 4984–4985.
10. Chen, S.; Ferreira, P. J.; Sheng, W. C.; Yabuuchi, N.; Allard, L. F.; Shao-Horn, Y. Enhanced Activity for Oxygen Reduction Reaction on "Pt_3CO" Nanoparticles: Direct Evidence of Percolated and Sandwich-Segregation Structures. *J. Am. Chem. Soc.* **2008**, *130*, 13818–13819.
11. Choi, S.-I.; Xie, S.; Shao, M.; Odell, J. H.; Lu, N.; Peng, H.-C.; Protsailo, L.; Guerrero, S.; Park, J.; Xia, X.; Wang, J.; Kim, M. J.; Xia, Y. Synthesis and Characterization of 9 nm Pt−Ni Octahedra with a Record High Activity of 3.3 A/mgPtfor the Oxygen Reduction Reaction. *Nano Lett.* **2013**, 3420–3425.
12. Khan, N. A.; Zellner, M. B.; Chen, J. G. Cyclohexene as a Chemical Probe of the Low-Temperature Hydrogenation Activity of Pt/Ni(111) Bimetallic Surfaces. *Surf. Sci.* **2004**, *556*, 87–100.
13. Chen, J. G.; Qi, S. T.; Humbert, M. P.; Menning, C. A.; Zhu, Y. X. Rational Design of Low-Temperature Hydrogenation Catalysts: Theoretical Predictions and Experimental Verification. *Acta Phys. Chim. Sin.* **2010**, *26*, 869–876.
14. Su, H. Y.; Bao, X. H.; Li, W. X. Modulating the Reactivity of Ni-Containing Pt(111)-Skin Catalysts by Density Functional Theory Calculations. *J. Chem. Phys.* **2008**, *128*, 194701.
15. Mu, R. T.; Fu, Q. A.; Xu, H.; Zhang, H. I.; Huang, Y. Y.; Jiang, Z.; Zhang, S. O.; Tan, D. L.; Bao, X. H. Synergetic Effect of Surface and Subsurface Ni Species at Pt−Ni Bimetallic Catalysts for CO Oxidation. *J. Am. Chem. Soc.* **2011**, *133*, 1978–1986.
16. Komatsu, T.; Tamura, A. Pt_3Co and PtCu Intermetallic Compounds: Promising Catalysts for Preferential Oxidation of CO in Excess Hydrogen. *J. Catal.* **2008**, *258*, 306–314.
17. Li, B. T.; Kado, S.; Mukainakano, Y.; Miyazawa, T.; Miyao, T.; Naito, S.; Okumura, K.; Kunimori, K.; Tomishige, K. Surface Modification of Ni Catalysts with Trace Pt for Oxidative Steam Reforming of Methane. *J. Catal.* **2007**, *245*, 144–155.
18. Besenbacher, F.; Chorkendorff, I.; Clausen, B. S.; Hammer, B.; Molenbroek, A. M.; Norskov, J. K.; Stensgaard, I. Design of a Surface Alloy Catalyst for Steam Reforming. *Science* **1998**, *279*, 1913–1915.
19. Hasche, F.; Oezaslan, M.; Strasser, P. Activity, Structure, and Degradation of Dealloyed $PtNi_3$ Nanoparticle Electrocatalyst for the Oxygen Reduction Reaction in PEMFC. *J. Electrochem. Soc.* **2012**, *159*, B25–B34.
20. Oezaslan, M.; Hasché, F.; Strasser, P. *In Situ* Observation of Bimetallic Alloy Nanoparticle Formation and Growth Using High-Temperature XRD. *Chem. Mater.* **2011**, *23*, 2159–2165.
21. Liu, Z.; Yu, C.; Rusakova, I.; Huang, D.; Strasser, P. Synthesis of Pt_3Co Alloy Nanocatalyst *via* Reverse Micelle for Oxygen Reduction Reaction in PEMFCs. *Top. Catal.* **2008**, *49*, 241–250.
22. Ahmadi, T. S.; Wang, Z. L.; Green, T. C.; Henglein, A.; ElSayed, M. A. Shape-Controlled Synthesis of Colloidal Platinum Nanoparticles. *Science* **1996**, *272*, 1924–1926.
23. Scott, R. W.; Datye, A. K.; Crooks, R. M. Bimetallic Palladium−Platinum Dendrimer-Encapsulated Catalysts. *J. Am. Chem. Soc.* **2003**, *123*, 3708–3709.
24. Liu, C.; Wu, X.; Klemmer, T.; Shukla, N.; Yang, X.; Weller, D. Polyol Process Synthesis of Monodispersed FePt Nanoparticles. *J. Phys. Chem. B* **2004**, *108*, 6121–6123.
25. Colon-Mercado, H. R.; Kim, H.; Popov, B. N. Durability Study Of Pt_3Ni_1 Catalysts as Cathode in PEM Fuel Cells. *Electrochem. Commun.* **2004**, *6*, 795–799.
26. Wei, Z. D.; Guo, H. T.; Tang, Z. Y. Heat Treatment of Carbon-Based Powders Carrying Platinum Alloy Catalysts for Oxygen Reduction: Influence on Corrosion Resistance and Particle Size. *J. Power Sources* **1996**, *62*, 233–236.
27. Gasteiger, H. A.; Kocha, S. S.; Sompalli, B.; Wagner, F. T. Activity Benchmarks and Requirements for Pt, Pt-Alloy, and non-Pt Oxygen Reduction Catalysts for PEMFCs. *Appl. Catal., B* **2005**, *56*, 9–35.
28. Salgado, J. R. C.; Antolini, E.; Gonzalez, E. R. Structure and Activity of Carbon-Supported Pt-Co Electrocatalysts for Oxygen Reduction. *J. Phys. Chem. B* **2004**, *108*, 17767–17774.
29. Ferreira, P. J.; la O', G. J.; Shao-Horn, Y.; Morgan, D.; Makharia, R.; Kocha, S.; Gasteiger, H. A. Instability of Pt/C Electrocatalysts in Proton Exchange Membrane Fuel Cells—A Mechanistic Investigation. *J. Electrochem. Soc.* **2005**, *152*, A2256–A2271.
30. Bindra, P.; Clouser, S. J.; Yeager, E. Platinum Dissolution in Concentrated Phosphoric Acid. *J. Electrochem. Soc.* **1979**, *126*, 1631–1632.
31. Strasser, P. Dealloyed Core Shell Fuel Cell Electrocatalysts. *Rev. Chem. Eng.* **2009**, *25*, 255–295.
32. Yang, R. Z.; Strasser, P.; Toney, M. F. Dealloying of Cu_3Pt (111) Studied by Surface X-ray Scattering. *J. Phys. Chem. C* **2011**, *115*, 9074–9080.
33. Gan, L.; Heggen, M.; Rudi, S.; Strasser, P. Core-Shell Compositional Fine Structures of Dealloyed Pt_xNi_{1-x} Nanoparticles and Their Impact on Oxygen Reduction Catalysis. *Nano Lett.* **2012**, *12*, 5423–5430.
34. Pourovskii, L. V.; Ruban, A. V.; Johansson, B.; Abrikosov, I. A. Antisite-Defect-Induced Surface Segregation in Ordered NiPt Alloy. *Phys. Rev. Lett.* **2003**, *90*, 026105.
35. Dahmani, C. E.; Cadeville, M. C.; Sanchez, J. M.; Moranlopez, J. I. Ni-Pt Phase-Diagram—Experiment and Theory. *Phys. Rev. Lett.* **1985**, *55*, 1208–1211.
36. Wang, G.; Van Hove, M. A.; Ross, P. N.; Baskes, M. I. Monte Carlo Simulations of Segregation in Pt−Ni Catalyst Nanoparticles. *J. Chem. Phys.* **2005**, *122*, 024706.
37. Oezaslan, M.; Hasché, F.; Strasser, P. *In Situ* High Temperature X-ray Diffraction Study of $PtCu_3$ Alloy Electrocatalyst for PEMFC. *Z. Anorg. Allg. Chem.* **2010**, *636*, 2111–2111.
38. Ghosh, T.; Leonard, B. M.; Zhou, Q.; DiSalvo, F. J. Pt Alloy and Intermetallic Phases with V, Cr, Mn, Ni, and Cu: Synthesis as Nanomaterials and Possible Applications As Fuel Cell Catalysts. *Chem. Mater.* **2010**, *22*, 2190–2202.

39. Wang, D.; Xin, H. L.; Hovden, R.; Wang, H.; Yu, Y.; Muller, D. A.; DiSalvo, F. J.; Abruña, H. D. Structurally Ordered Intermetallic Platinum–Cobalt Core–Shell Nanoparticles with Enhanced Activity and Stability as Oxygen Reduction Electrocatalysts. *Nat. Mater.* **2013**, *12*, 81–87.
40. Lozovoi, A. Y.; Alavi, A.; Finnis, M. W. Surface Stoichiometry and the Initial Oxidation of NiAl(110). *Phys. Rev. Lett.* **2000**, *85*, 610–613.
41. Khan, N. A.; Zellner, M. B.; Murillo, L. E.; Chen, J. G. A Comparison of Similarities and Differences in the Activities of Pt/Ni(111) and Ni/Pt(111) Surfaces. *Catal. Lett.* **2004**, *95*, 1–6.
42. Skoplyak, O.; Menning, C. A.; Barteau, M. A.; Chen, J. G. Reforming of Oxygenates for H_2 Production on 3d/Pt(111) Bimetallic Surfaces. *Top. Catal.* **2008**, *51*, 49–59.
43. Skoplyak, O.; Menning, C. A.; Barteau, M. A.; Chen, J. G. Experimental and Theoretical Study of Reactivity Trends for Methanol on Co/Pt(111) and Ni/Pt(111) Bimetallic Surfaces. *J. Chem. Phys.* **2007**, *127*, 114707.
44. Gasteiger, H. A.; Markovic, N. M. Just a Dream or Future Reality?. *Science* **2009**, *324*, 48–49.
45. Humbert, M. P.; Chen, J. G. Correlating Hydrogenation Activity with Binding Energies of Hydrogen and Cyclohexene on M/Pt(111) (M = Fe, Co, Ni, Cu) Bimetallic Surfaces. *J. Catal.* **2008**, *257*, 297–306.
46. Nashner, M. S.; Frenkel, A. I.; Somerville, D.; Hills, C. W.; Shapley, J. R.; Nuzzo, R. G. Core Shell Inversion During Nucleation and Growth of Bimetallic Pt/Ru Nanoparticles. *J. Am. Chem. Soc.* **1998**, *120*, 8093–8101.
47. Wang, G.; Vanhove, M.; Ross, P.; Baskes, M. Quantitative Prediction of Surface Segregation in Bimetallic Pt–M Alloy Nanoparticles (M = Ni, Re, Mo). *Prog. Surf. Sci.* **2005**, 28–45.
48. Cui, C.; Ahmadi, M.; Behafarid, F.; Gan, L.; Neumann, M.; Heggen, M.; Roldan Cuenya, B.; Strasser, P. Shape-Selected Bimetallic Nanoparticle Electrocatalysts: Evolution of Their Atomic-Scale Structure, Chemical Composition, and Electrochemical Reactivity under Various Chemical Environments. *Faraday Discuss.* **2013**, 91–112.
49. Cui, C.; Gan, L.; Heggen, M.; Rudi, S.; Strasser, P. Compositional Segregation in Shaped Pt Alloy Nanoparticles and Their Structural Behaviour During Electrocatalysis. *Nat. Mater.* **2013**, 765–771.
50. Wu, Y.; Cai, S.; Wang, D.; He, W.; Li, Y. Syntheses of Water-Soluble Octahedral, Truncated Octahedral, and Cubic Pt–Ni Nanocrystals and Their Structure–Activity Study in Model Hydrogenation Reactions. *J. Am. Chem. Soc.* **2012**, *134*, 8975–8981.
51. Menning, C. A.; Chen, J. G. Thermodynamics and Kinetics of Oxygen-Induced Segregation of 3d Metals in Pt-3d-Pt(111) and Pt-3d-Pt(100) Bimetallic Structures. *J. Chem. Phys.* **2008**, *128*, 164703.
52. Menning, C. A.; Chen, J. G. General Trend for Adsorbate-Induced Segregation of Subsurface Metal Atoms in Bimetallic Surfaces. *J. Chem. Phys.* **2009**, *130*, 174709.
53. Mu, R. T.; Fu, Q.; Liu, H. Y.; Tan, D. L.; Zhai, R. S.; Bao, X. H. Reversible Surface Structural Changes in Pt-Based Bimetallic Nanoparticles During Oxidation and Reduction Cycles. *Appl. Surf. Sci.* **2009**, *255*, 7296–7301.
54. Yang, D. Q.; Sacher, E. Interaction of Evaporated Nickel Nanoparticles with Highly Oriented Pyrolytic Graphite: Back-Bonding to Surface Defects, as Studied by X-ray Photoelectron Spectroscopy. *J. Phys. Chem. B* **2005**, *109*, 19329–19334.
55. Behafarid, F.; Roldan Cuenya, B. Coarsening Phenomena of Metal Nanoparticles and The Influence of the Support Pre-Treatment: Pt/TiO_2(110). *Surf. Sci.* **2012**, *606*, 908–918.
56. Jak, M. J. J.; Konstapel, C.; van Kreuningen, A.; Chrost, J.; Verhoeven, J.; Frenken, J. W. M. The Influence of Substrate Defects on the Growth Rate of Palladium Nanoparticles on a TiO_2(110) Surface. *Surf. Sci.* **2001**, *474*, 28–36.
57. Belton, D. N.; Sun, Y. M.; White, J. M. Metal-Support Interactions on Rhodium and Platinum/Titanium Dioxide Model Catalysts. *J. Phys. Chem.* **1984**, *88*, 5172–5176.
58. Park, J. B.; Conner, S. F.; Chen, D. A. Bimetallic Pt-Au Clusters on TiO_2(110): Growth, Surface Composition, and Metal-Support Interactions. *J. Phys. Chem. C.* **2008**, *112*, 5490–5500.
59. Porsgaard, S.; Ono, L. K.; Zeuthen, H.; Knudsen, J.; Schnadt, J.; Merte, L. R.; Chevallier, J.; Helveg, S.; Salmeron, M.; Wendt, S.; Besenbacher, F. *In Situ* Study of CO Oxidation on HOPG-Supported Pt Nanoparticles. *ChemPhysChem* **2013**, 1553–1557.
60. Croy, J. R.; Mostafa, S.; Liu, J.; Sohn, Y.-h.; Roldan Cuenya, B. Size-Dependent Study of MeOH Decomposition Over Size-Selected Pt Nanoparticles Synthesized *via* Micelle Encapsulation. *Catal. Lett.* **2007**, *118*, 1–7.
61. Porsgaard, S.; Merte, L. R.; Ono, L. K.; Behafarid, F.; Matos, J.; Helveg, S.; Salmeron, M.; Roldan Cuenya, B.; Besenbacher, F. Stability of Platinum Nanoparticles Supported on SiO_2/Si(111): A High-Pressure X-ray Photoelectron Spectroscopy Study. *ACS Nano* **2012**, 10743–10749.
62. Dai, W. L.; Qiao, M. H.; Deng, J. F. XPS Studies on a Novel Amorphous Ni-Co-W-B Alloy Powder. *Appl. Surf. Sci.* **1997**, *120*, 119–124.
63. Grunthaner, P. J.; Grunthaner, F. J.; Mayer, J. W. XPS Study of the Chemical-Structure of the Nickel–Silicon Interface. *J. Vac. Sci. Technol.* **1980**, *17*, 924–929.
64. Grosvenor, A. P.; Biesinger, M. C.; Smart, R. S.; McIntyre, N. S. New Interpretations of XPS Spectra of Nickel Metal and Oxides. *Surf. Sci.* **2006**, *600*, 1771–1779.
65. Li, F. B.; Li, X. Z. The Enhancement of Photodegradation Efficiency Using Pt-TiO_2 Catalyst. *Chemosphere* **2002**, *48*, 1103–1111.
66. Rajalakshmi, N.; Ryu, H.; Shaijumon, M. M.; Ramaprabhu, S. Performance of Polymer Electrolyte Membrane Fuel Cells with Carbon Nanotubes as Oxygen Reduction Catalyst Support Material. *J. Power Sources* **2005**, *140*, 250–257.
67. Wen, Y. N.; Zhang, H. M. Surface Energy Calculation of the Fcc Metals by Using the MAEAM. *Solid State Commun.* **2007**, *144*, 163–167.
68. Deng, L.; Hu, W.; Deng, H.; Xiao, S.; Tang, J. Au–Ag Bimetallic Nanoparticles: Surface Segregation and Atomic-Scale Structure. *J. Phys. Chem. C* **2011**, *115*, 11355–11363.
69. Cheng, D.; Yuan, S.; Ferrando, R. Structure, Chemical Ordering, and Thermal Stability of Pt–Ni Alloy Nanoclusters. *J. Phys.: Condens. Matter* **2013**, *25*, 1–9.
70. Abrikosov, I.; Ruban, A.; Skriver, H.; Johansson, B. Calculated Orientation Dependence of Surface Segregations in $Pt_{50}Ni_{50}$. *Phys. Rev. B* **1994**, *50*, 2039–2042.
71. Oezaslan, M.; Heggen, M.; Strasser, P. Size-Dependent Morphology of Dealloyed Bimetallic Catalysts: Linking the Nano to the Macro Scale. *J. Am. Chem. Soc.* **2012**, *134*, 514–524.
72. Heggen, M.; Oezaslan, M.; Houben, L.; Strasser, P. Formation and Analysis of Core–Shell Fine Structures in Pt Bimetallic Nanoparticle Fuel Cell Electrocatalysts. *J. Phys. Chem. C* **2012**, *116*, 19073–19083.
73. Li, W.; Österlund, L.; Vestergaard, E.; Vang, R.; Matthiesen, J.; Pedersen, T.; Lægsgaard, E.; Hammer, B.; Besenbacher, F. Oxidation of Pt(110). *Phys. Rev. Lett.* **2004**, *93*, 146104.
74. Kwon, S. G.; Hyeon, T. Formation Mechanisms of Uniform Nanocrystals *via* Hot-Injection and Heat-Up Methods. *Small* **2011**, *7*, 2685–2702.
75. http://www.casaxps.com.
76. Xu, C. X.; Liu, Y. Q.; Zhou, C.; Wang, L.; Geng, H. R.; Ding, Y. An *In Situ* Dealloying and Oxidation Route to Co_3O_4 Nanosheets and Their Ambient-Temperature CO Oxidation Activity. *ChemCatChem* **2011**, *3*, 399–407.
77. Schubert, M. M.; Kahlich, M. J.; Feldmeyer, G.; Huttner, M.; Hackenberg, S.; Gasteiger, H. A.; Behm, R. J. Bimetallic PtSn Catalyst for Selective CO Oxidation in H_2-Rich Gases at Low Temperatures. *Phys. Chem. Chem. Phys.* **2001**, *3*, 1123–1131.
78. Stamenkovic, V.; Arenz, M.; Blizanac, B. B.; Mayrhofer, K. J. J.; Ross, P. N.; Markovic, N. M. *In Situ* CO Oxidation on Well Characterized Pt_3Sn(hkl) Surfaces: A Selective Review. *Surf. Sci.* **2005**, *576*, 145–157.